Acta Materialia 232 (2022) 117936

Contents lists available at ScienceDirect

Acta Materialia

journal homepage: www.elsevier.com/locate/actamat

Precipitate dissolution during deformation induced twin thickening in a CoNi-base superalloy subject to creep

Vassili A. Vorontsov[a], Thomas P. McAuliffe[b], Mark C. Hardy[c], David Dye[b], Ioannis Bantounas[b,*]

[a] Department of Design, Manufacturing and Engineering Management, University of Strathclyde, James Weir Building, 75 Montrose Street, Glasgow, G1 1XJ, UK
[b] Department of Materials, Imperial College, South Kensington, London SW7 2AZ, UK
[c] Rolls-Royce plc, Derby, DE24 8BJ, UK

ARTICLE INFO

Article history:
Received 6 December 2021
Revised 8 April 2022
Accepted 11 April 2022

Keywords:
Cobalt-base superalloys
Creep
Microtwinning
Atomic ordering
Transmission electron microscopy

ABSTRACT

The tensile creep performance of a polycrystalline Co/Ni-base superalloy with a multimodal γ' distribution has been examined at 800°C and 300 MPa. The rupture life of the alloy is comparable to that of RR1000 tested under similar conditions. Microstructural examination of the alloy after testing revealed the presence of continuous γ' precipitates and $M_{23}C_6$ carbides along the grain boundaries. Intragranularly, coarsening of the secondary γ' precipitates occurred at the expense of the fine tertiary γ'. Long planar deformation bands, free of γ', were also observed to traverse individual grains. Examination of the deformation bands confirmed that they were microtwins. Long sections of the microtwins examined were depleted of γ' stabilising elements across their entire width, suggesting that certain alloy compositions are susceptible to precipitate dissolution during twin thickening. A mechanism for the dissolution of the precipitates is suggested based on the Kolbe reordering mechanism.

1. Introduction

The development of γ/γ' two phase Co- and CoNi-based superalloys is promising for improved performance of high temperature structural applications. The exceptional high temperature performance of Ni-based superalloys is attributed to the precipitation of a coherent $L1_2$ ordered γ' phase within a disordered face centred cubic γ matrix. The shearing resistance offered by these ordered precipitates results in the excellent creep resistance they display.

The discovery of a γ/γ' two phase field within the Co-Al-W ternary system [1,2] has enabled the development of Co- and CoNi-based superalloys for high temperature applications [3–6]. Traditionally, Ni-based superalloys are used for structural applications where a combination of good strength, environmental resistance and creep strength are of importance [7,8]. Understanding of creep behaviour is critical to the implementation of Co- and CoNi-base superalloys for high performance applications. Promising single crystal CoNi-base superalloys have been developed with comparable creep resistance to that of 1st generation Ni-base superalloys [9,10].

Microtwinning has been observed in Ni-base [11–16] and CoNi-base [17] superalloys tested between temperatures of 650–750 °C and stresses of 350–850 MPa. Though twinning is typically associated with high strain rate deformation at low temperatures [18,19], these microtwins form at intermediate temperatures under slow strain rates. Knowles and Chen[13] have suggested that microtwins nucleate from superlattice extrinsic stacking faults (SESFs).

Several mechanisms have been suggested for the creation of such faults [13,20–25], the reader is referred to Unocic et al. [26] for a comprehensive review. However, diffraction contrast experiments [14] and high resolution TEM micrographs [17,27] have confirmed the presence of $\frac{1}{6}$<112> dislocations at the leading edge of extended stacking faults on adjacent {111} planes. Such an observation would require dislocation decorrelation [28] and suggests that the likely twinning mechanism is that suggested by Kolbe [24]. Shearing of the $L1_2$ superlattice by $\frac{1}{6}$<112> Shockley partials results in the formation of a pseudo twin [29]. In such a configuration the order of the $L1_2$ superlattice is not preserved across the twin boundary. Kolbe [24] suggested that a “true” twin structure could be restored via a two step atomic re-ordering process involving the short range diffusion of atomic species in the wake of the leading partials.

* Corresponding author.
E-mail address: ibantounas.ac@gmail.com (I. Bantounas).

https://doi.org/10.1016/j.actamat.2022.117936

In addition to short range atomic re-ordering, long range diffusion of γ stabilising elements have been shown to segregate to the leading partials [30–32]. This Cottrell atmosphere is thought to lower the energy penalty associated with forming a complex stacking fault (CSF) when shearing the γ' via $\frac{1}{6}$<112> partials [33] and is considered as the rate limiting step during twin formation [30]. Segregation of γ stabilising elements is not restricted to the leading partials but has also been observed at the fault boundaries [17,34–36], an observation not limited to the Ni- and CoNi-base alloy systems but having also been reported in MnAl Heusler alloys [37] and Mg alloys [38]. In some alloy systems, segregation of elements to stacking faults can stabilise new phases within the fault [35,39–41]. Examples include the η phase in a variant of the Ni-base superalloy ME3 [39] and the DO_{19} phase in the Co-Al-W-Ta system [40].

Precipitation of carbides after prolonged high temperature exposure has been reported in polycrystalline and single crystal Ni-base superalloys [42–46]. In Cr rich alloys aged at intermediate temperatures, $M_{23}C_6$ carbides precipitate with a cube-cube orientation relationship with the parent matrix [45,47]. Carbides are commonly associated with regions of localised deformation and, together with grain boundaries, are thought to be dislocation nucleation sites [28,48,49]. In the present work, we propose such carbides to be the sources of twinning.

In this paper a γ/γ' CoNi-base superalloy with a bimodal γ/γ' size distribution has been creep tested to rupture at 800°C and 300 MPa. Examination of the post-test microstructure revealed the presence of precipitate-free bands which traversed entire γ grains. These bands were confirmed to be deformation-induced twins which are thought to nucleate at the incoherent interface of grain boundary $M_{23}C_6$ carbides. It is postulated that the ordered precipitates dissolve into the γ matrix during thickening of the twin. A mechanism for the dissolution of the precipitates is proposed and the consequences of these structures discussed within the text. To our knowledge, this is the first report of precipitate dissolution during twin growth in superalloys.

2. Experimental

A CoNi-base superalloy designated V208C, developed by Knop et al. [50], was melted in a vacuum arc-melter backfilled with argon and poured into a 23 × 23×60 mm mould. Table 1 shows the nominal alloy composition. The ingot was homogenised in a vacuum furnace at 1250°C for 48 h and profile rolled at 1200°C down to a 13 × 13 mm cross section with a maximum of 15% strain per pass. Samples were machined into creep specimens with a 14.8 mm gauge length and 5 mm gauge diameter. Annular ridges were machined on enlarged shoulders of the test specimen for attaching an extensometer. Creep specimens were encapsulated in quartz tubes under low pressure argon and solution treated at 1100°C for 1 h, slow cooled at 20°C/min to 700°C and air cooled (AC) to room temperature (RT). The specimen was further aged at 825°C for 4 h followed by AC to RT.

The grain size of the alloy was 33±4 μm, including twins, as measured from optical micrographs using the Abrams three circle method outlined in ASTM E112.32609. Average equivalent area diameter of the secondary and tertiary γ' precipitates were measured using ImageJ software. The γ'_s and γ'_t sizes were 100 and 22 nm, respectively.

Table 1
Nominal compositions (at. %) and γ' area fraction of alloy V208C (Patent Ref. [51]).

Co	Ni	Cr	Al	W	Ta	C	B	Zr	γ' fract.
36.1	34	15	10.5	3	1	0.15	0.2	0.04	52%

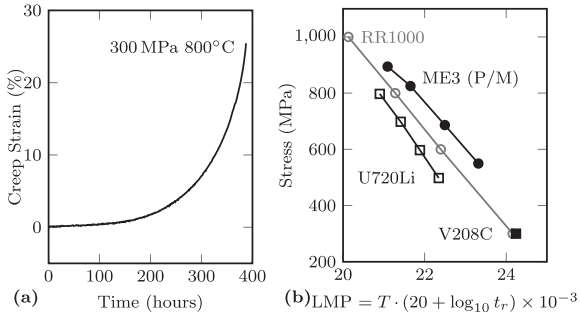

Fig. 1. (a) Creep curve of specimen tested in tension at 800°C and 300 MPa, and (b) comparison of creep performance with U720Li [54], RR1000 [55] and ME3 [56] on a Larson Miller parameter graph.

Creep tests were performed in tension on a lever-loading machine under a constant force to rupture.[1] The test temperature was set to 800°C and the starting stress to 300 MPa. Two thermocouples attached with high temperature wire to the centre of the gauge were used to monitor temperature during testing. Creep strain was recorded by fitting an extensometer to the annular ridges on the test piece. The change in displacement was measured using a transducer attached to a pair of arms extending below the furnace.

The deformed microstructure was examined by sectioning the gauge perpendicular to the loading direction. Samples were progressively ground down to 4000 grit SiC paper and then polished using a suspension containing 100 ml water, 30ml coloidal silica suspension and 70ml H_2O_2. The γ' precipitates were revealed by electroetching in a solution of 2.5% phosphoric acid in methanol using a voltage of 10V for 10 seconds. Transmission electron microscopy (TEM) lamellae were prepared from the polished cross-section using an FEI Helios Nanolab 600 focussed ion beam workstation via the *in-situ* lift-out technique [52,53]. The twin chemistry was examined in a JEOL JEM-2100F microscope equipped with a XEDS silicon-drift detector from Oxford Instruments. XEDS data was collected and analysed using the Oxford Instruments AZTec v3.1 software package. Electron micrographs were acquired with the InLens detector on Zeiss Sigma 300 and a Zeiss Auriga CrossBeam scanning electron microscopes. The secondary electron images presented were acquired on a FEI Helios Nanolab 600 workstation.

3. Results

3.1. Creep behaviour

The tensile creep strain vs time curve for the alloy tested at 800°C and 300 MPa is shown in Fig. 1(a). The time to rupture was 390 h with a minimum creep rate of 8.6E-9 s^{-1}. Fig. 1(b) shows the test results displayed on a Larson-Miller parameter (LMP) plot, Eq. (1).

$$\mathrm{LMP} = T \cdot (20 + \log_{10} t_r) \times 10^{-3}\,, \tag{1}$$

where T is the test temperature in Kelvin and t_r the time to rupture in hours.

The graph compares the current alloy to the performance of industrially relevant disk alloys U720Li [54], RR1000 [55] and

[1] The test was paused and restarted after 360 h (≈16% strain) as the displacement limit of the test apparatus was reached. This involved removing the load from the specimen, cooling to room temperature and re-adjusting the aparatus prior to restarting the test. At this point, the material was within the tertiary creep regime with 30 h remaining to rupture.

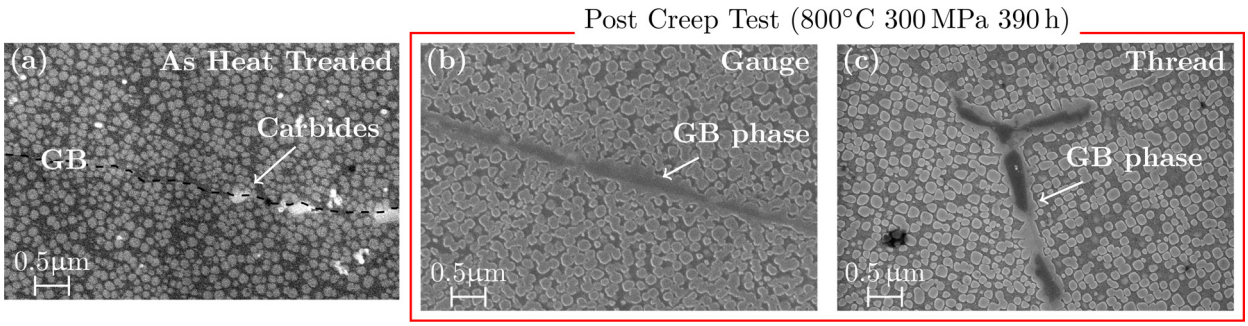

Fig. 2. InLens micrographs showing (a) grain boundary carbides in the pre-test microstructure, (b) and (c) growth of continuous grain boundary phases post creep test at 800°C for 390 h in the specimen gauge and thread, respectively.

ME3 (P/M) [56]. At a stress of 300 MPa V208C in the current microstructural condition has a comparable LMP to that of RR1000 [55], a disk superalloy currently used in gas turbine engines.

3.2. Grain boundary evolution

Exposing the alloy to a temperature of 800°C for 390 h precipitated out Cr rich $M_{23}C_6$ carbides and γ' at the γ grain boundaries. The grain boundary structure before creep testing is shown in Fig. 2(a). A dashed line is drawn on the micrograph to outline the boundary, as there is little contrast to distinguish it from the bulk of the two adjacent grains. Few carbides can be seen decorating the boundary. The post creep test microstructure is shown in Fig. 2(b,c). Micrographs from the gauge section after exposure at 800°C and 300 MPa for 390 h reveal the presence of phases decorating the grain boundaries of the alloy, Fig. 2(b). These phases are also observed within the microstructure from the threads of the specimen, Fig. 2(c), implying that they are not stress induced phases but rather a result of heat treatment during testing.

The grain boundary phases which formed after testing are Cr rich $M_{23}C_6$ carbides and the $L1_2$ γ' phase. Fig. 3(a) shows a centre beam dark field (CBDF) conventional (C)TEM micrograph of a foil prepared from the gauge of the creep specimen. Two grains labelled G1 and G2 are visible in the top left and bottom right of the micrograph, respectively. Grain G2 is oriented along the [001] zone axis, Fig. 3(c), with a superlattice reflection selected for the CBDF micrograph. The γ' precipitates appear bright against a dark γ matrix, while grain G1 does not contribute to the image and appears dark. A carbide is located along the grain boundary, more clearly visible in the centre beam dark field (CBDF) micrograph in Fig. 3(b). The carbide is oriented along the [001] zone axis and its crystal structure resembles that of $M_{23}C_6$, Fig. 3(d).

Scanning transmission electron microscopy (STEM) energy dispersive spectroscopy (EDS) maps reveal that the carbide from Fig. 3(b) is enriched in Cr, Fig. 3(f). Additionally, the carbide is surrounded by γ' precipitates and bound between two Ta/Zr rich carbides. The compositions of the Cr and Ta/Zr-rich carbides are presented in Table 2.

The Cr enrichment coupled with the large cubic lattice parameter suggests that this is an $M_{23}C_6$ carbide with approximate composition $Cr_{23}C_6$. The space group of this phase is classified as $Fm\bar{3}m$ in Hermann-Mauguin notation. In turn, Ta/Zr-rich carbides tend to be MC carbides. The formation of $M_{23}C_6$ and γ' at the grain boundaries after prolonged exposure to high temperature is due to the decomposition of MC grain boundary carbides according to the $MC + \gamma \rightarrow M_{23}C_6 + \gamma'$ reaction sequence [7,8].

Table 2
Carbide compositions (at. %) measured via STEM-EDS.

Phase	Co	Ni	Al	W	Ta	Cr	C	Zr
$M_{23}C_6$	6	2	0	3	0	75	13	0
MC	5	2	0	4	24	31	26	9

3.3. Carbide induced slip

Our results suggest that the growth of $M_{23}C_6$ follows a cube-cube relationship with one of the grains while inducing strain and the nucleation of slip bands in the adjacent grain, Fig. 4. A selected area diffraction pattern (SADP) of grain G2 imaged along the $[001]_\gamma$ zone is shown in Fig. 3(c), a SADP of the $M_{23}C_6$ carbide which shares a cube-cube relationship with this grain is shown in Fig. 3(d). A SADP of both the carbide and γ grain are presented in Fig. 3(e). These diffraction patterns clearly display the orientation relationship between the carbide and matrix. A CBDF micrograph of the carbide which shares a relationship with grain G2 is provided in Fig. 3(b). This carbide is labelled as "$M_{23}C_6$||G2" in Fig. 4(a,c), denoting it's cube-cube orientation relationship with grain G2, and is connected to a deformation twin in the adjacent grain G1. Likewise, carbide "$M_{23}C_6$||G1" shares a cube-cube relationship with grain G1 and is connected to a deformation band in the adjacent grain G2.

All characterisation of deformation in this study was performed after the specimen was crept to failure. The deformation associated with carbides was thus not observed whilst in the process of initiating but after testing.

We can infer that the carbides nucleate and form a semi-coherent interface with the grain they share an orientation relationship with while exerting a strain on the adjacent grain with which they share an incoherent interface during growth. Coupled with the load from the creep test, these incoherent interfaces make for favourable sites for the initiation of slip events. Delaying the precipitation of these carbides could thus prolong the creep life of the alloy.

3.4. Microstructural evolution

A bimodal γ' microstructure consisting of coarse secondary and finer tertiary precipitates was obtained after heat treating the rolled ingot. The microstructure is presented in Fig. 5(a). It consists of secondary γ' precipitates with a mean diameter of 100 nm and 22 nm tertiary precipitates. The seconary and tertiary precipitate area fractions were 49 and 3%, respectively. After creep testing the secondary γ' precipitates coarsen and coalesce at the expense of the tertiary, Fig. 5(b). In addition, bands free of precipitates which traverse entire γ grains are observed. These bands, later shown to be deformation microtwins, are the focus of subsequent sections.

3.5. Deformation microstructure

Fig. 6 (a) shows a section of the microstructure of the crept specimen taken from the gauge perpendicular to the loading direc-

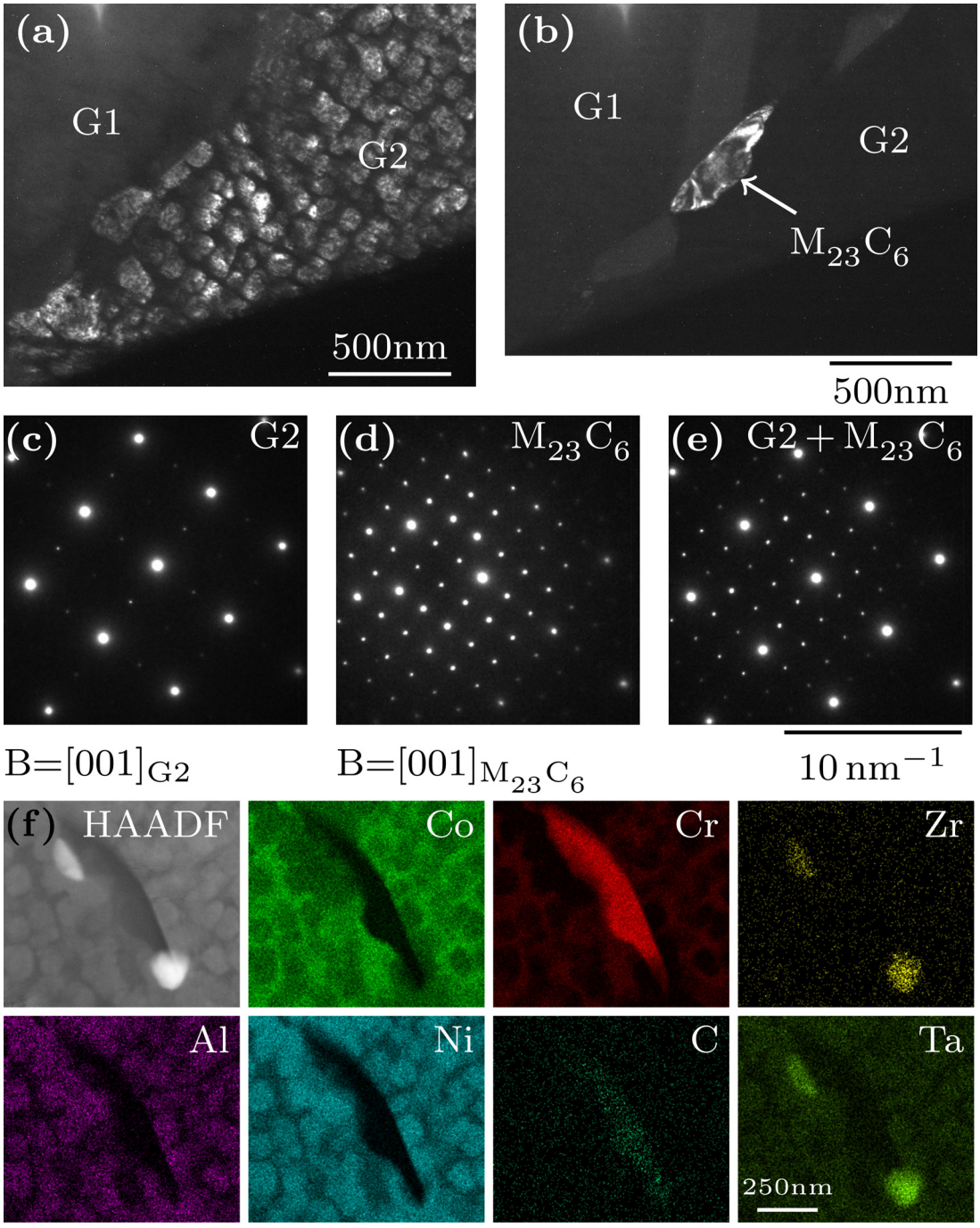

Fig. 3. CBDF micrographs from grain G2 showing (a) intragrannular and grain boundary γ' precipitates and (b) grain boundary $M_{23}C_6$ carbide coherent with grain G2. SADPs from (c) the bulk of grain G2 and (d) the $M_{23}C_6$ carbide. (e) SADP showing the cube-cube orientation relationship between G2 and the $M_{23}C_6$ carbide. All SADPs imaged along the [001] beam direction. (f) STEM HAADF micrograph of carbide with accompanying EDS maps. All micrographs acquired from gauge of creep specimen tested at 300 MPa and 800°C for 390 h.

tion. The arrows indicate precipitate free bands. These bands end at grain boundaries. Grain boundary γ' and Cr rich $M_{23}C_6$ carbides, characterised in the previous section, can also be seen to decorate the grain boundary.

A magnified view of the grain interior showing a deformation band is displayed in Fig. 6(b). The figure highlights the abscence of precipitates within the band. In order to characterise the deformation and chemical structure of the band, a TEM foil was extracted from a deformed grain. Fig. 6(c) shows the location of the TEM lamella prior to FIB milling. The area was selected in order to encompass multiple bands within the foil.

Conventional transmission electron microscopy reveals that these deformation bands are deformation twins on the order of a few hundred nanometers in thickness. A selected area diffraction pattern (SADP) from an area containing the precipitate free bands is shown in Fig. 7(a). The foil is oriented such that the beam direction is along the [011] zone axis of the grain. Along this zone, diffuse diffraction spots can be seen about the $(\bar{1}\bar{1}1)$ plane, revealing the twin nature of the precipitate free bands.

A $[\bar{2}00]$ matrix reflection was selected to create a centre beam dark field (CBDF) micrograph in Fig. 7(b). The parent grain is bright and the deformation bands dark. Fig. 7 is a CBDF micrograph using

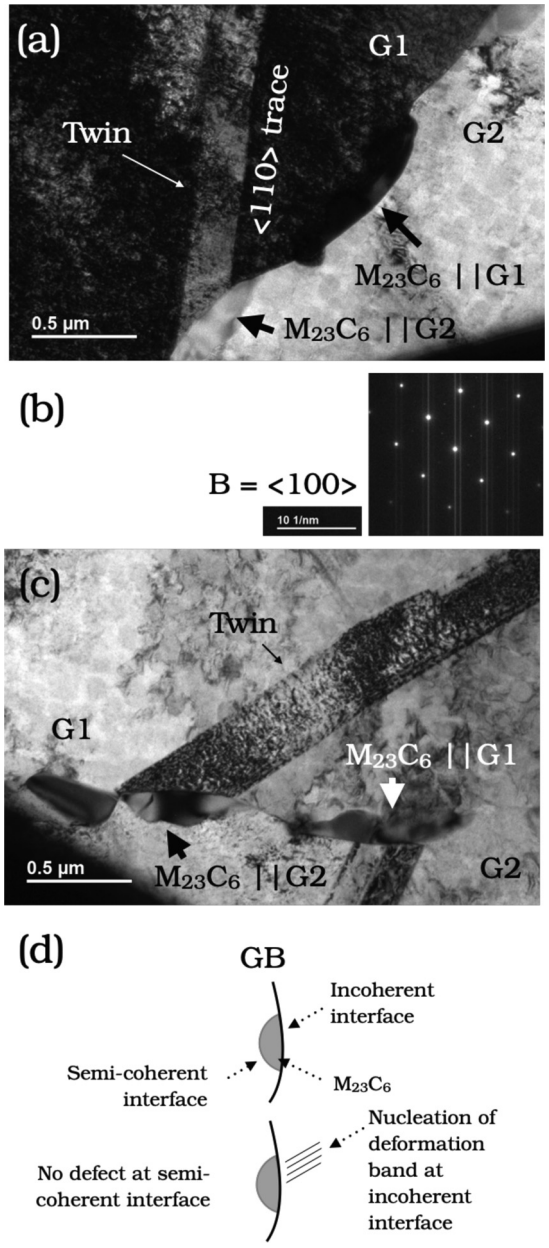

Fig. 4. (a) BF TEM micrograph taken along the <100> zone axis of grain G1 and carbide $M_{23}C_6$||G1 showing deformation twin intersect the foil plane along the <110> trace. (b) SADP from (a) - Note that the vertical streaks in the DP are due to charging of the CCD camera and do not reflect a property of the material. (c) BF TEM micrograph showing deformation twin in G1 ending at grain boundary carbide labelled $M_{23}C_6$||G2 which shares a cube-cube relationship with grain G2 and an incoherent interface with G1. (d) Schematic showing defect nucleation at an incoherent interface as a result of grain boundary $M_{23}C_6$ carbide precipitation and growth.

a $[1\bar{1}1]$ twin reflection. In this instance the parent grain appears dark and the twin structure bright. These micrographs confirm that the deformation bands observed in the SEM are deformation twins. Consistent with the absence of γ' precipitates observed in the SEM micrographs, no superlattice reflections can be observed from the twinned reflections. Despite the lack of superlattice reflections the chemical compsition of the twin suggests regions of high concentration of γ' stabilising elements.

The sample in this study was tested to rupture with a strain to failure of approximately 25%. We estimate that the creep strain due to twinning in this material varies between 1% and 8%, with a mean value of 4%, Appendix A.

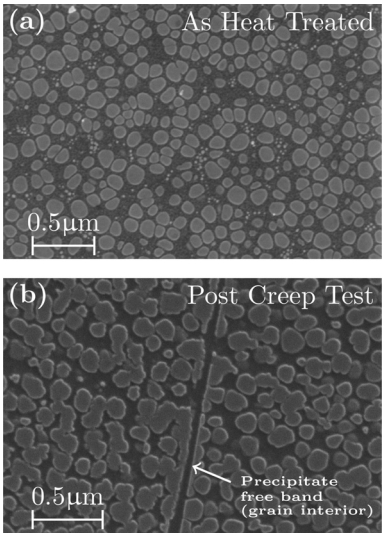

Fig. 5. InLens micrographs of (a) the as-heat treated microstructure showing the secondary and tertiary γ' precipitates, and (b) post-test microstructure from the gauge showing coarsening and coalescence of secondary γ' along with precipitate-free bands within the grain interior.

3.6. Twin chemistry

Consistent with the majority of observed deformation twins from SEM micrographs the twin channels are enriched in γ stabilising elements, as shown via STEM-XEDS maps in Fig. 8(b). The X-ray maps show the distribution of Co, Cr, Ni and Al within two twinned regions. In this alloy, Co and Cr partition to the γ phase while Ni and Al partition to the γ' phase [50]. Despite the SEM micrographs revealing an absence of γ' precipitates within the deformation channels, the elemental maps show concentrations of γ' stabilising elements coupled with regions rich in γ stabilising elements. The composition of elements across the twin in both such cases is examined next.

Line profiles across the thickness of the twin are presented from regions rich in γ' and γ stabilising elements, Fig. 8(a) and (b), respectively. We first examine the case of a twinned region containing a γ' precipitate, or more specifically, a region rich in Ni and Al γ' stabilising elements, referred to as Case A and depicted in Fig. 8(a). Tracking the Ni K_α quantitative line profile from left to right shows a decrease in concentration to a minimum of $\approx$ 24 at.% followed by a rise to $\approx$ 36 at.%. This first dip is believed to be due to the converged electron beam crossing from a $\gamma+\gamma'$ region of the foil to a γ channel, the composition of which is consistent with atom probe tomography results of the γ phase in this alloy [50]. The beam then scans across a $\gamma+\gamma'$ region of the foil, which becomes progressively richer in γ'. Following the peak in Ni composition of $\approx$ 36 at.% there is a dip in concentration of $\approx$ 6 at.% Ni at the twin/matrix interface. The Ni concentration increases throughout the thickness of the twin to $\approx$ 34 at.%, however does not recover to the composition of the undeformed precipitate. A second dip in the concentration is again observed at the adjacent twin/matrix interface. After the electron beam crosses this planar interface the Ni concentration gradually decreases from a $\gamma+\gamma'$ phase region to that of pure γ. The Al K_α line profile follows a similar trend to that of Ni, both elements preferentially partitioning to the γ' phase.

Line profiles of X-ray peaks from the γ stabilisers, Co K_α and Cr K_α, follow an inverse pattern to that of Ni and Al. The concentration of Co and Cr gradually decreases as the electron beam moves from the γ channel to a region containing $\gamma+\gamma'$ phases. At the twin/matrix interfaces the concentration of γ stabilising elements

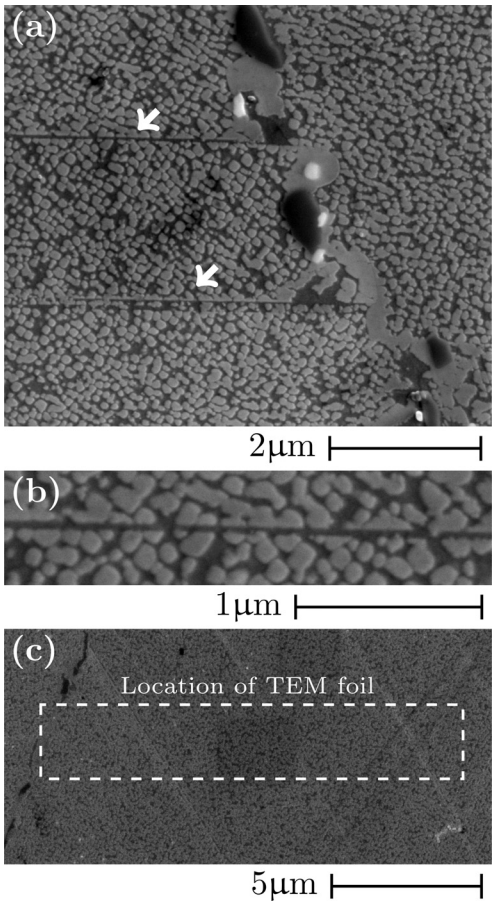

Fig. 6. Secondary electron micrographs showing (a) precipitate free bands (white arrows) terminating at a grain boundary, (b) magnified view of precipitate free bands from the grain interior, and (c) location of TEM foil encompassing multiple bands.

increases. A schematic of the precipitate and twin configuration is depicted in Fig. 8(c) where a twin is confined within a γ' precipitate with its twin/matrix interfaces depleted in γ' and enriched in γ stabilising elements. This is attributed to long range diffusion of γ stabilising elements during twin lengthening through a γ' precipitate [31,32] and helps to lower the energy penalty associated with the passage of $\frac{1}{6}$<112> partials on adjacent {111} planes during twin thickening [17]. Across the thickness of the twin the elemental composition does not recover to that of the γ'. The authors believe this is thus converted to a disordered γ phase enriched in γ' stabilisers.

A different scenario is presented in Fig. 8(b) where the composition across the entire thickness of the twin resembles that of the γ phase (Case B). Tracking the Ni K_α line profile. The concentration of Ni gradually increases from $\approx$ 26 at.% in the γ phase, to $\approx$ 39 at.% as it enters a $\gamma+\gamma'$ phase region. A sudden drop to $\approx$ 26 at.% is observed at the twin/matrix interface. Up to this point, this observation is consistent with the previous case when the twin is contained within a γ' precipitate. However, unlike the previous example, the concentration of Ni does not recover to that of the γ' precipitate but remains low at $\approx$ 25 at.%, resembling that of the γ phase, throughout the thickness of the twin. As the converged beam crosses the adjacent twin/matrix interface the concentration of Ni sharply rises again by $\approx$ 5 at.% and then follows a gradual increase to $\approx$ 34 at.% before gradually decreasing to $\approx$ 27 at.%. The raised Ni concentration on either side of the twin is thought to be two separate γ' precipitates. The Al K_α peak follows a similar trend to that of Ni, while the Co and Cr K_α peaks, being γ stabilisers, follow an inverse pattern. I.e., deplete when the electron beam scans the γ' precipitate and increase in the twin region.

In this instance we believe that the twin has nucleated (i.e. lengthened) within the γ matrix and consumed the adjacent γ' precipitates during the thickening stage of its life. A schematic is shown in Fig. 8(d) to depict the migration of γ stabilising elements to the prior precipitate boundary. This creates a region along the length of the twin depleted in γ' stabilising elements with a composition very close to that of the γ phase which stretches across the entirity of its width. A mechanism is proposed in the disussion for the creation of such a twinned region.

4. Discussion

4.1. Carbide precipitation and slip

We propose that the precipitation of $M_{23}C_6$ carbides at the grain boundaries introduces strain in the adjacent grain which, coupled with the load from the creep test, make the carbides favourable areas for slip nucleation. The work from Section 3.2 clearly shows grain boundary $M_{23}C_6$ carbides precipitating coherently with one of the grains adjacent to the grain boundary. Fig. 4(c) shows two $M_{23}C_6$ carbides precipitating coherently with one of the grains and evidence of slip at the boundary between the carbide and the adjacent grain. Carbide $M_{23}C_6$||G1 shares a cube-cube orientation relationship with grain G1. The car-

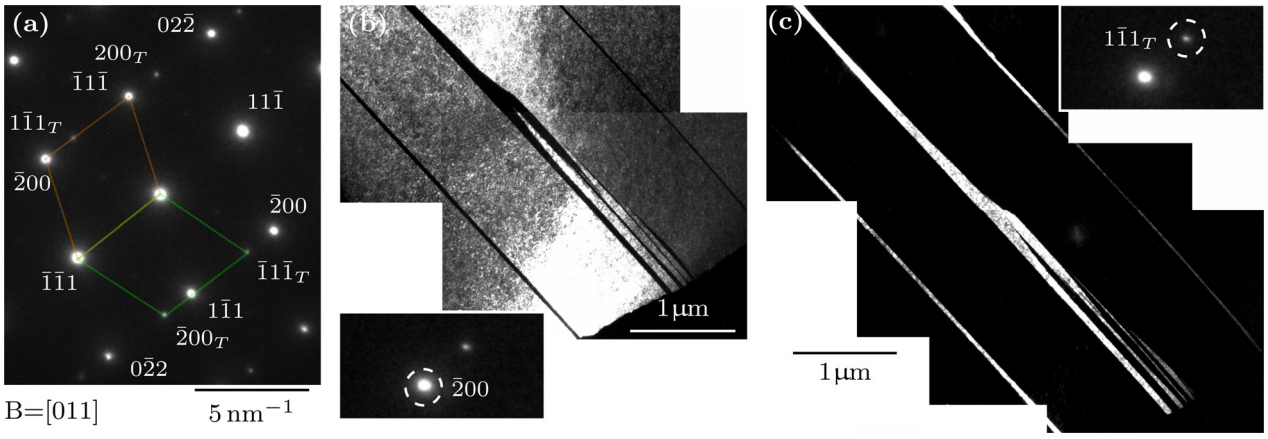

Fig. 7. (a) Selected area diffraction pattern along the [110] zone showing twin reflections (marked with a 'T' subscript), and centre beam dark field micrographs from (b) matrix [$\bar{2}$00] beam with twins appearing dark and (c) twin $[1\bar{1}1]_T$ reflection with twins appearing bright.

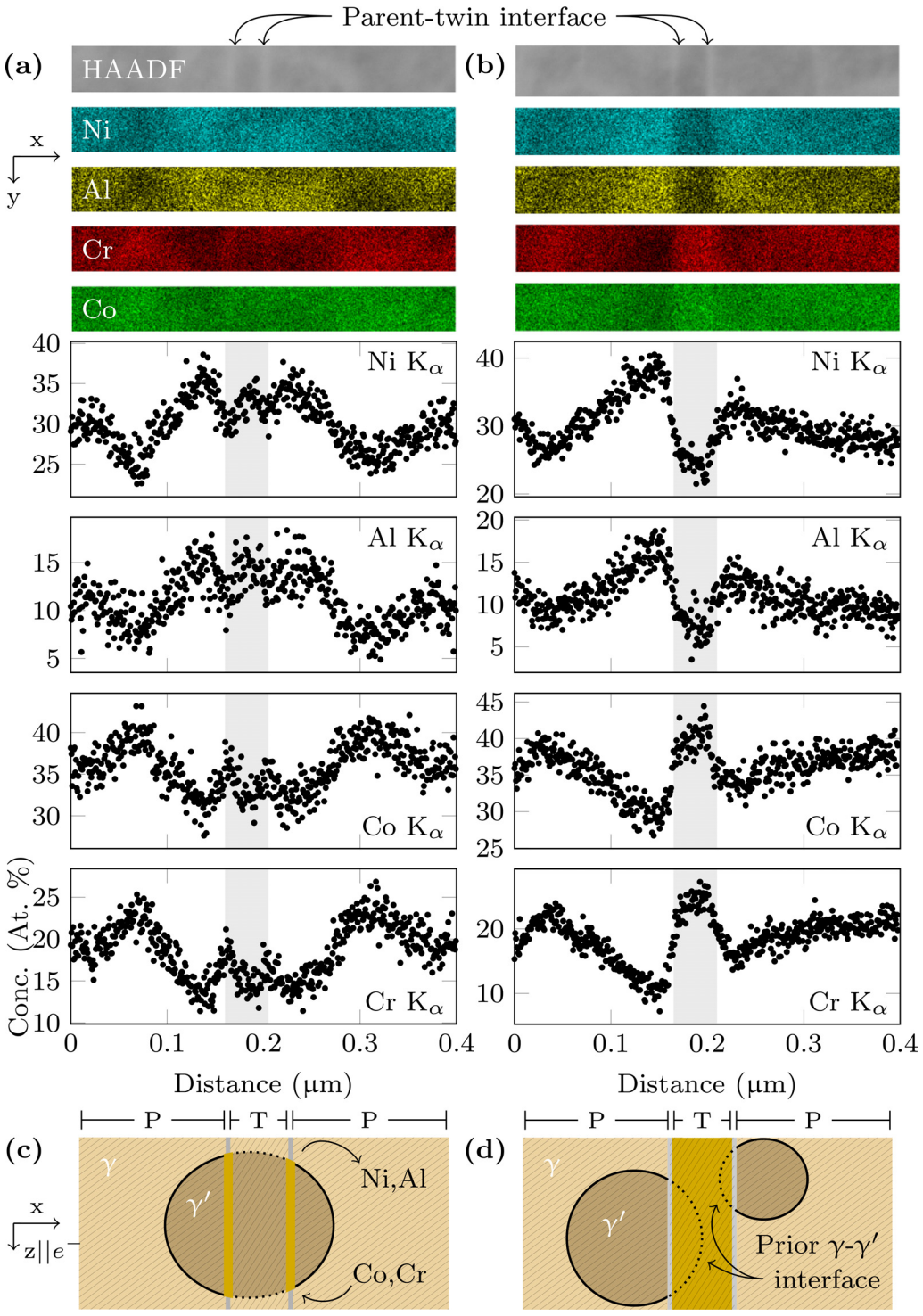

Fig. 8. X-ray line profiles across thickness of twin showing (a) enrichment of γ and depletion of γ' stabilising elments at twin/matrix interface when the twin is confined within a γ' precipitate - Case A, (b) consumption of γ' precipitates by γ stabilising elements during twin thickening - Case B. Schematics (c) and (d) show the physical representations of the line profile observations from (a) and (c), respectively. Hashed lines represent the $(\bar{1}01)$ planes. 'P' and 'T' in the schematics denote regions of the parent and twin, respectively.

bide shares a semi-coherent interface with this grain while its interface with the adjacent grain G2 is incoherent. A deformation twin is seen to lie on the adjacent grain G2 intersecting grain G1 at the incoherent interface of the $M_{23}C_6$||G1 carbide. The same can be observed for carbide $M_{23}C_6$||G2 which has a cube-cube orientation relationship with G2 and shows evidence of slip in the adjacent grain G1. It is stressed, however, that these are not direct observations of defect initiation but inferences of the sort. A schematic depicting these observations is presented in Fig. 4(d).

In support of the above argument, SEM micrographs from the threads of the creep specimen reveal that stress is not a prerequisite for the formation of these grain boundary carbides, Fig. 2(c). This means that in trying to understand the spacial coincidence of the carbide and deformation structure we are lead to believe that

the defects are not a prerequisite for carbide nucleation but that likely the opposite is true. Carbides precipitate at the grain boundaries due to thermodynamics and act as nucleation sites for the deformation structures.

The implication of this observation is that there could be room to improve the creep performance of this alloy by lowering the Cr additions. Grain boundary $M_{23}C_6$ is stabilised by chromium. Reducing chromium could suppress the formation of the grain boundary carbide during exposure to high temperature. If the carbides indeed act as slip initiation sites for twin formation, as discussed above, their suppression could also delay the onset of such deformation. This in turn would prolong the time to rupture and improve the creep performance of the alloy. Given the comparable performance of this alloy with RR1000 [55], a Ni-base superalloy in current use in jet engines, there is therefore potential for polycrystalline CoNi-base superalloys to outperform current generation disk Ni-base superalloys.

4.2. Twinning mechanism

In this study we are concerned with twin growth and the observation of long regions of precipitate-free twins. Two mechanisms are proposed for twin growth based on the presence of γ' precipitates within the vicinity of the original twin. Both cases can be accounted for by the following example.

A single twin is nucleated from a SF that has grown across both the γ and γ' phases from one end of a grain to the other. Across the length of the fault both phases have undergone a displacement. As the twin thickens perpendicular to the {111} twin plane it carries with it the segregation of γ stabilising elements. When the twin is confined to one γ' precipitate, Case A shown in Fig. 8(c), the twin boundaries are enriched in Co and Cr and depleted in Ni and Al, with the region between the boundaries being a disordered γ phase enriched in γ' stabilising elements. In instances where the twin has nucleated within the disordered γ matrix and continues to thicken in the direction of an ordered γ' precipitate, once the twin boundary reaches the adjacent precipitate instead of cutting into the precipitate, dissolution of the precipitate occurs, Case B in Fig. 8(d). The twin boundary consumes the neighbouring precipitate.

4.3. Proposed precipitate dissolution mechanism

4.3.1. Case B: twin thickening from the γ matrix into a γ' precipitate

As the twin boundary moves by the motion of $\frac{1}{3}$<112> partials gliding on adjacent {111} planes, the twin thickens one atomic plane at a time, Fig. 9(a). If the twin is locally contained within a region of disordered γ phase there will come a time during the thickening process were the twin boundary will interact with a γ/γ' interface, Fig. 9(b). The $\frac{1}{3}$<112> partial is a $\frac{1}{6}$<112> superlattice partial in γ'. Shearing of the first {111} γ' atomic layer by the superlattice partial creates a single layer pseudo-twin within the γ' precipitate. If this pseudo-twin was in the bulk of the precipitate atomic reordering with atoms from an adjacent {111} plane would convert it to a true twin structure. However, in the current case we are presented with a single layer pseudo-twin boundary on one side of the planar fault and a γ/γ' interface at the other, Fig. 9(c). We hypothesise that such a configuration is thermodynamically unstable at the testing temperature of 800°C and so the single layer pseudo-twin would disorder, via atomic reshuffling with the γ phase, dissolving into the γ matrix, Fig. 9(d). This results in a γ/γ' twin boundary as observed in the present work.

4.3.2. Case A: twin thickening confined within a γ' precipitate

SEM micrographs suggest the dissolution of the ordered precipitates across the thickness of the twins. With a few exceptions,

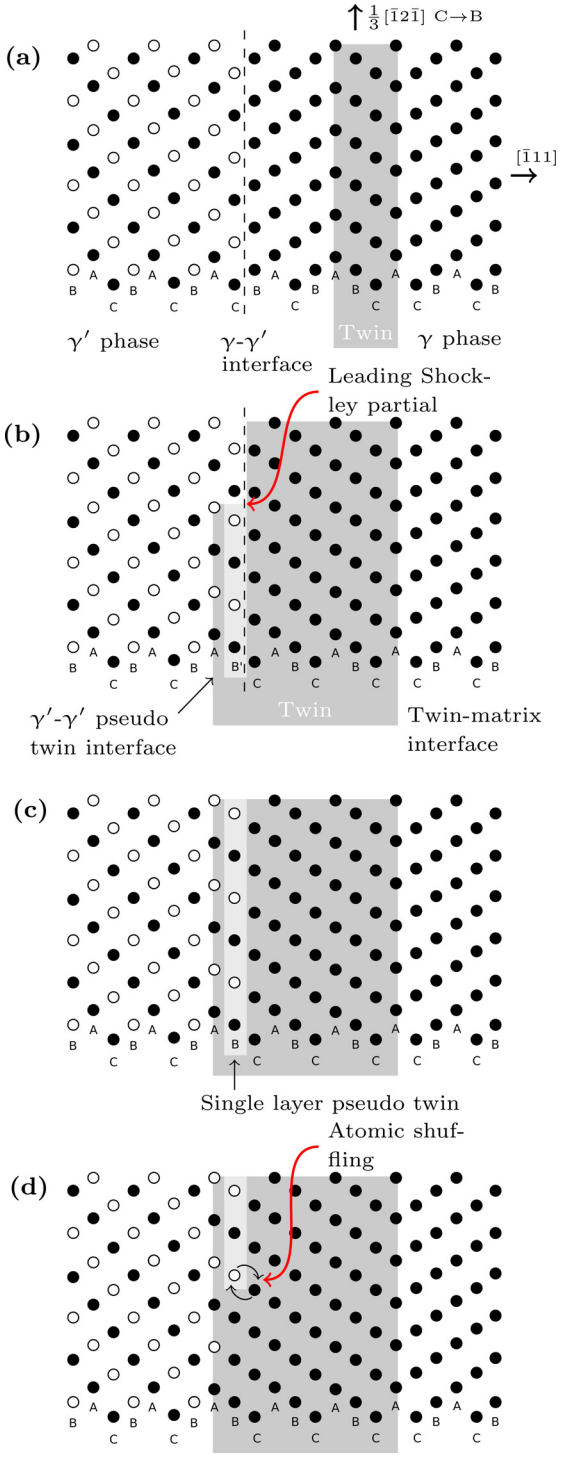

Fig. 9. Schematic showing formation of a single layer pseudo twin at a $\gamma - \gamma'$ interface and consequent precipitate dissolution. (a) Twin within the γ matrix, dark grey region. (b) Twin growth into the first γ' atomic layer showing creation of a single layer pseudo twin in the wake of the leading Schockley partial, light grey region. (c) The partial has made its way across a narrow stretch of the $\gamma - \gamma'$ interface leaving behind it a single layer pseudo twin. A parent-twin γ'-psuedo twin interface is shown on the left and a pseudo twin matrix on the right. (d) Atomic shuffling in the wake of the leading Shockley partial disorders the single layer pseudo twin slowly dissolving the γ' precipitate during the process of twin growth.

where precipitates appear to show shear marks along the twin boundaries, the majority of cases show no evidence of the precipitate between the twin boundaries. Initially we thought this to be due to a difference in the starting position of the embryonic twin

in relation to the ordered precipitate boundary. Areas where the twin lengthened within the disordered γ phase and consequently thickened into an ordered γ' precipitate dissolve the precipitate (case B). Cases where the embryonic twin fault lengthens within a γ' precipitate and consequently thickens within the precipitate would retain the γ' order across the fault thickness while showing segregation of γ stabilising elements along the fault boundaries (case A). The latter case having been reported in the literature and being the now 'typical' observation when studying microtwinning in superalloys. We put typical in inverted commas as this is still an evolving area with new findings being brought to light with a healthy cadence.

With the introduction of these two mechanisms, dependent on the initial position of the lengthening fault, we could account for the variability in our STEM-XEDS observations. Areas where the composition across the twin thickness was that of the γ phase (case B) and areas where the composition was closer to that of the γ' (slightly depleted) with enrichment of γ elements at the fault boundaries (case A). This interpretation, however, has one drawback. The likelihood of an embryonic twin fault starting out in the γ phase across the majority of its length is very small given the γ' area fraction in this alloy and cannot account for the length of the precipitate free twins in our SEM observations. We are thus required to rethink our hypothesis.

Taking a step back, it is clear we have indirectly inferred that the material between the planar twin faults for case A has maintained the γ' structure from its chemical composition. STEM-XEDS results, however, only provide data on elemental species, not their atomic arrangements. We can thus rethink our hypothesis on the basis that this region is not a region of ordered γ' with a slightly depleted composition but rather a region of disordered γ enriched in γ' stabilising elements. Looking at case A in this light we can draw the following mechanism for its formation.

Following along the lines of Barba et al. [31] microtwins develop from complex stacking faults (CSFs) when $\frac{1}{2} < 110 >$ dislocations dissociate into $\frac{1}{6} < 112 >$ Shockley partials shear the γ' (step 1). This high energy CSFs can not propagate far into the ordered precipitate. Co and Cr then partition to the leading partial, lowering the energy of the CSF (step 2). At the same time short range reordering at the wake of the leading partials creates an embryonic microtwin (step 3). The process leaving behind traces of the partitioned elements along the fault plane. As the twin thickens, via successive shearing of adjacent {111} planes, the partitioned elements aid in the propagation of the fault (step 4). The final structure being a twin contained within a γ' precipitate with Co and Cr segregation along the fault planes (step 5). It is worth noting that there is no explanation as to how the order of the precipitate, as well as its composition, regain that of the original γ' as the twin thickens.

Our reasoning follows a similar pattern with the exception that the twinned region is disordered with a composition tending toward γ. Steps 1 to 4 are the same as above. In step 4, however, the segregation of γ formers to the fault boundary transform the fault to a "γ-like region" as described by Smith et al. [57] for the Ni-base superalloy ME3. In the present case this segregation of γ formers is enough to locally disorder the γ'. As the twin thickens the order is not restored in its wake. Instead the resulting structure is one where the twin boundaries tend toward a γ composition and the twin thickness is comprised of a disordered matrix with a composition ever so slightly richer in γ' formers than the twin boundaries. One can also imagine that once the thickness of the disordered twin reaches a certain limit, the mechanism for case B can be adopted for its propagation, refer to section 4.3.1 above.

The above hypothesis gives a better account of the SEM observations. It also raises two important questions which challenge it. If the segregation of γ formers locally disorder the fault boundary what is the driving force for their segregation upon twin thickening? I.e. how can we account for the segregation of γ formers at the fault boundary once it is no longer sandwiched between an ordered precipitate phase. And secondly, why do the γ' formers not segregate away from the precipitate once disordered? I.e. why don't they dissolve into the matrix and form a homogeneous solution?

4.4. Practical significance

Such a mechanism is important for two reasons. (i) The layer-by-layer dissolution process of the ordered precipitate phase at the γ/γ' twin interface may be a rate limiting step for twin thickening. (ii) The formation of precipitate free bands which traverse entire γ grains can provide resistance-free dislocation paths, which, in turn increase creep rates and result in large strains at grain boundaries. This may be more prevalent during a transition to a high stress low temperature creep regime where twin motion is not favoured and dislocations glide free from the resistance of ordered precipitates along previously formed twins.

5. Summary and conclusions

The tensile creep performance of a polycrystalline Co/Ni-base superalloy processed so as to produce a multimodal γ' distribution has been examined at 800°C and 300 MPa. The main findings are as follows:

- The rupture life of the alloy is similar to that of commercial alloy RR1000 tested under the same conditions.
- $M_{23}C_6$ carbides nucleate at γ grain boundaries during creep. These carbides observe a cube-cube orientation relationship with the grain which they share a semi-coherent interface with, while acting as defect nucleation sites in the adjacent grain with which they share an incoherent interface.
- γ' precipitate-free twins are observed to cross large regions of γ grains. Solute segregation at the γ/γ' phase boundary is suggested to result in the dissolution of the precipitate as the twin grows from the dissordered matrix phase into the ordered precipitate, slowly consuming the precipitate and creating a twin predominantly free of the ordered γ' phase. This mechanisms is similar to the Kolbe re-ordering with the exception that in the classical mechanism the pseudo twin is contained within the ordered precipitate whereas in the present case it is sandwiched between the ordered precipitate and the disordered matrix phase.

These findings suggest that polycrystalline Co/Ni-base superalloys have the potential to compete with commercial Ni-base superalloys in terms of creep performance. Precipitation of $M_{23}C_6$ carbides act as defect nucleation sites at the incoherent carbide-matrix interface, and that the composition of the V208C Co/Ni-base superalloy is prone to precipitate dissolution during twin growth when creep tested in tension at 800°C and 300 MPa.

Declaration of Competing Interest

The authors declare that they have no known competing financial interests or personal relationships that could have appeared to influence the work reported in this paper

Acknowledgment

This work was funded under the Rolls-Royce-EPSRC strategic partnership in structural metallic systems for gas turbines (EP/M005607/1). The authors would like to thank Dr Catrin Davies and Alex Toth from the Mechanical Engineering Department at

Imperial College London for help with the use of the creep rigs within the High Temperature Testing laboratory. Our thanks is also extended to Mike Lennon and Ben Wood for their assistance in creep specimen preparation. VAV would like to acknowledge support from Rolls-Royce plc and Imperial College London under the Imperial College Research Fellowship scheme.

Appendix A. Calculation of strain due to twinning

Contrast in the TEM micrographs suggests a high density of dislocations within the matrix, which could be carrying the majority of the load. As such, it is interesting to ask what role twinning plays as the operative deformation mechanism within this creep condition. To answer this we first note that the strain to failure was approximately 25% with the transition from secondary to tertiary creep regimes occurring below 1% creep strain.

Follow the reasoning used by Viswanathan et al [14], we make an attempt to measure the strain due to twinning as they provide a permanent marker for shear displacement. Assuming the twinning partials are of the type 1/6<112> (as shown in [14]) the displacement due to a single twin can be expressed in terms of the twin thickness, n, as

$$\Delta = n \cdot a_0(\sqrt{6}/6). \tag{A1}$$

Where n is the twin thickness expressed as the number of {111} planes.

In the current work we have not used high resolution TEM to directly measure the twin thickness in terms of the number of {111} planes, n, as done in Viswanathan et al. [14]. Instead we have to formulate an equation to calculate n as a function of the twin thickness along the <111> direction, $t_{<111>}$, as measured from centre beam dark field TEM micrographs (e.g. Fig. 7(b) or (c) in our manuscript) and the lattice parameter a_0. We start by equating the number of {111} planes to the twin thickness along the [111] direction divided by the interplanar spacing of the (111) plane,

$$n = t_{[111]}/d_{(111)}. \tag{A2}$$

We then exploit the geometric relationship between a_0 and $d_{(111)}$ using the well known relationship $1/d_{hkl}^2 = 1/a_0^2 \cdot (h^2 + k^2 + l^2)$ for the interplanar spacing in cubic crystal lattices, where h, k, and l are the Miller indices of the plane in question. For the (111) plane this equation becomes

$$d_{111} = a_0/\sqrt{3}. \tag{A3}$$

We can substitute Eq. (A3) into Eq. (A2) to express the number of {111} planes in terms of a_0, $n = t_{[111]} \cdot \sqrt{3}/a_0$. Then further substitute this equation into Eq. (A1) to express the displacement due to a single twin in terms of the twin thickness along the <111> direction, $\Delta = t_{[111]} \cdot \sqrt{3} \cdot \sqrt{6}/6$, eliminating a_0 from the equation. This reduces to

$$\Delta = t_{[111]} \cdot \sqrt{18}/6. \tag{A4}$$

Viswanathan et al [14] then argue that the strain due to the twins, γ, can be expressed as the average displacement per twin, Δ_{av}, multiplied by the number of twins, N_{twins}, per unit length, L. The equation being

$$\gamma = \Delta_{av} \cdot N_{twins}/L. \tag{A5}$$

Using Eqs. (A4) and (A5) we can now express the strain as a function of the twin thickness along the <111> direction, enabling the use of TEM micrographs such as those in Fig. 7(b) and (c) for measuring $d_{[111]}$ and calculating γ. The calculated creep strain due to twinning in this material varies between 1 and 8%, with a mean value of 4%. The sample in this study was tested to rupture with a strain to failure of approximately 25%. The strain accommodated by twinning thus varies between 1/25th and 1/3rd of the total strain.

It is interesting to compare the strain due to twinning to the strain at which the material transitions between the secondary and tertiary creep regimes, creep strain less than 1% (between 0.50 and 0.75%). Though we are not in a position to answer this question with the current test specimen it is worth asking if the majority of the strain within primary and secondary creep regimes is accommodated by twinning. Further work with interrupted tests at strains of 0.1 and 0.25% could help answer this question and help us understand if the dissolution of precipitates during the twin thickening process have a role to play in influencing the creep rate.

References

[1] J. Sato, T. Omori, K. Oikawa, I. Ohnuma, R. Kainuma, K. Ishida, Cobalt-base high-temperature alloys, Science 312 (2006) 90–91, doi:10.1126/science.1121738.
[2] C.S. Lee, Precipitation-Hardening Characteristics of Ternary Cobalt - Aluminium - X Alloys, The University of Arizona, 1971. Ph.d. thesis doctoral.
[3] T.M. Pollock, J. Dibbern, M. Tsunekane, J. Zhu, A. Suzuki, New Co-based γ-γ′ high-temperature alloys, JOM 62 (1) (2010) 58–63, doi:10.1007/s11837-010-0013-y.
[4] A. Suzuki, H. Inui, T.M. Pollock, $L1_2$-strengthened cobalt-base superalloys, Annu. Rev. Mater. Res. 45 (2015) 345–368, doi:10.1146/annurev-matsci-070214-021043.
[5] S. Neumeier, L. Freund, M. Göken, Novel wrought γ/γ′ cobalt base superalloys with high strength and improved oxidation resistance, Scr. Mater. 109 (2015) 104–107, doi:10.1016/j.scriptamat.2015.07.030.
[6] A. Bauer, S. Neumeier, F. Pyczak, M. Goeken, Microstructure and creep strength of different gamma/gamma'-strengthened co-base superalloy variants, Scr. Mater. 63 (12) (2010) 1197–1200, doi:10.1016/j.scriptamat.2010.08.036.
[7] R.C. Reed, The Superalloys, Cambridge University Press, 2007.
[8] C.T. Sims, N.S. Stoloff, W.C. Hagel, Superalloys II, Wiley, Hoboken, NJ, 1987.
[9] M.S. Titus, A. Suzuki, T.M. Pollock, Creep and directional coarsening in single crystals of new – cobalt-base alloys, Scr. Mater. 66 (8) (2012) 574–577, doi:10.1016/j.scriptamat.2012.01.008.
[10] M.S. Titus, A. Suzuki, T.M. Pollock, High temperature creep of new $L1_2$ containing cobalt-base superalloys, in: Superalloys 2012, John Wiley & Sons, Inc., 2012, pp. 823–832, doi:10.1002/9781118516430.ch91.
[11] M.G. Ardakani, M. McLean, B.A. Shollock, Twin formation during creep in single crystals of nickel-based superalloys, Acta Mater. 47 (9) (1999) 2593–2602.
[12] K. Kakehi, Effect of primary and secondary precipitates on creep strength of Ni-base superalloy single crystals, Mater. Sci. Eng. A. 278 (1–2) (2000) 135–141.
[13] D. Knowles, Q. Chen, Superlattice stacking fault formation and twinning during creep in γ/γ' single crystal superalloy CMSX-4, Mat. Sci. Eng. A 340 (1) (2003) 88–102, doi:10.1016/S0921-5093(02)00172-7.
[14] G. Viswanathan, P. Sarosi, M. Henry, D. Whitis, W. Milligan, M. Mills, Investigation of creep deformation mechanisms at intermediate temperatures in René 88 DT, Acta Mater. 53 (10) (2005) 3041–3057, doi:10.1016/j.actamat.2005.03.017.
[15] S. Karthikeyan, R. Unocic, P. Sarosi, G. Viswanathan, D. Whitis, M. Mills, Modeling microtwinning during creep in Ni-based superalloys, Scr. Mater. 54 (6) (2006) 1157–1162, doi:10.1016/j.scriptamat.2005.11.049.
[16] T.M. Smith, R.R. Unocic, H. Deutchman, M.J. Mills, Creep deformation mechanism mapping in nickel base disk superalloys, Mater. High Temp. 33 (4–5) (2016) 372–383, doi:10.1080/09603409.2016.1180858.
[17] L.P. Freund, O.M.D.M. Messé, J.S. Barnard, M. Göken, S. Neumeier, C.M.F. Rae, Segregation assisted microtwinning during creep of a polycrystalline $L1_2$-hardenend co-base superalloy, Acta Mater. 123 (2017) 295–304, doi:10.1016/j.actamat.2016.10.048.
[18] G.E. Dieter, Mechanical metallurgy, McGraw-Hill Series in Materials Science and Engineering, 3rd, McGraw-Hill, New York; London, 1986.
[19] J.W. Christian, S. Mahajan, Deformation twinning, Prog. Mater. Sci. 39 (1–2) (1995) 1–157.
[20] B. Kear, A. Giamei, G. Leverant, J. Oblak, On intrinsic/extrinsic stacking fault pairs in the $L1_2$ lattice, Scr. Metall. 3 (2) (1969) 123–129, doi:10.1016/0036-9748(69)90214-2.
[21] M. Condat, B. Décamps, Shearing of γ' precipitates by single a/2 < 110 > matrix dislocations in a γ/γ' Ni-based superalloy, Scr. Metall. 21 (5) (1987) 607–612, doi:10.1016/0036-9748(87)90369-3.
[22] B. Décamps, A.J. Morton, M. Condat, On the mechanism of shear of gamma' precipitates by single (a/2)(110) dissociated matrix dislocations in Ni-based superalloys, Philos. Mag. A 64 (3) (1991) 641–668.
[23] B. Décamps, A.J. Morton, On the presence of fine matrix channels in Ni-based superalloys and their effect on shearing processes of gamma' precipitates, Philos. Mag. A 68 (6) (1993) 1129–1149.
[24] M. Kolbe, The high temperature decrease of the critical resolved shear stress in nickel-base superalloys, Mat. Sci. Eng. A 319–321 (2001) 383–387, doi:10.1016/S0921-5093(01)00944-3.
[25] B. Décamps, S. Raujol, A. Coujou, F. Pettinari-Sturmel, N. Clément, D. Locq, P. Caron, On the shearing mechanism of γ' precipitates by a single (a/6)<

112 > Shockley partial in Ni-based superalloys, Philos. Mag. 84 (1) (2004) 91–107, doi:10.1080/14786430310001621472.
[26] R.R. Unocic, G.B. Viswanathan, P.M. Sarosi, S. Karthikeyan, J. Li, M.J. Mills, Mechanisms of creep deformation in polycrystalline Ni-base disk superalloys, Mater. Sci. Eng. A 483–484 (2008) 25–32, doi:10.1016/j.msea.2006.08.148.
[27] L. Koravik, R.R. Unocic, J. Li, M.J. Mills, The intermediate temperature deformation of Ni-based superalloys: importance of reordering, JOM 61 (2009) 42–48.
[28] R.R. Unocic, N. Zhou, L. Kovarik, C. Shen, Y. Wang, M.J. Mills, Dislocation decorrelation and relationship to deformation microtwins during creep of a γ' precipitate strengthened Ni-based superalloy, Acta Mater. 59 (2011) 7325–7339, doi:10.1016/j.actamat.2011.07.069.
[29] J.W. Christian, D.E. Laughlin, The deformation twinning of superlattice structures derived from disordered BCC or FCC solid-solutions, Acta Metall. Mater. 36 (7) (1988) 1617–1642.
[30] T.M. Smith, Y. Rao, Y. Wang, M. Ghazisaeidi, M.J. Mills, Diffusion processes during creep at intermediate temperatures in a Ni-based superalloy, Acta Mater. 141 (2017) 261–272, doi:10.1016/j.actamat.2017.09.027.
[31] D. Barba, S. Pedrazzini, A. Vilalta-Clemente, A.J. Wilkinson, M.P. Moody, P.A.J. Bagot, A. Jerusalem, R.C. Reed, On the composition of microtwins in a single crystal nickel-based superalloy, Scr. Mater. 127 (2017) 37–40, doi:10.1016/j.scriptamat.2016.08.029.
[32] D. Barba, E. Alabort, S. Pedrazzini, D.M. Collins, A.J. Wilkinson, P.A.J. Bagot, M.P. Moody, C. Atkinson, A. Jerusalem, R.C. Reed, On the microtwinning mechanism in a single crystal superalloy, Acta Mater. 135 (2017) 314–329, doi:10.1016/j.actamat.2017.05.072.
[33] Y. Rao, T.M. Smith, M.J. Mills, M. Ghazisaeidi, Segregation of alloying elements to planar faults in gamma'-Ni_3Al, Acta Mater. 148 (2018) 173–184, doi:10.1016/j.actamat.2018.01.055.
[34] G.B. Viswanathan, R. Shi, A. Genc, V.A. Vorontsov, L. Kovarik, C.M.F. Rae, M.J. Mills, Segregation at stacking faults within the gamma' phase of two Ni-base superalloys following intermediate temperature creep, Scripta Mater. 94 (2015) 5–8, doi:10.1016/j.scriptamat.2014.06.032.
[35] M.S. Titus, A. Mottura, G.B. Viswanathan, A. Suzuki, M.J. Mills, T.M. Pollock, High resolution energy dispersive spectroscopy mapping of planar defects in $L1_2$-containing Co-base superalloys, Acta Mater. 89 (2015) 423–437, doi:10.1016/j.actamat.2015.01.050.
[36] Y.M. Eggeler, J. Müller, M.S. Titus, A. Suzuki, T.M. Pollock, E. Spiecker, Planar defect formation in the γ' phase during high temperature creep in single crystal CoNi-base superalloys, Acta Mater. 113 (2016) 335–349.
[37] D. Palanisamy, D. Raabe, B. Gault, Elemental segregation to twin boundaries in a MnAl ferromagnetic Heusler alloy, Scr. Mater. 155 (2018) 144–148, doi:10.1016/j.scriptamat.2018.06.037.
[38] J.F. Nie, Y.M. Zhu, J.Z. Liu, X.Y. Fang, Periodic segregation of solute atoms in fully coherent twin boundaries, Science 340 (6135) (2013) 957–960, doi:10.1126/science.1229369.
[39] T.M. Smith, B.D. Esser, N. Antolin, G.B. Viswanathan, T. Hanlon, A. Wessman, D. Mourer, W. Windl, D.W. McComb, M.J. Mills, Segregation and η phase formation along stacking faults during creep at intermediate temperatures in a Ni-based superalloy, Acta Mater. 100 (2015) 19–31, doi:10.1016/j.actamat.2015.08.053.
[40] M.S. Titus, R.K. Rhein, P.B. Wells, P.C. Dodge, G.B. Viswanathan, M.J. Mills, A. Van der Ven, T.M. Pollock, Solute segregation and deviation from bulk thermodynamics at nanoscale crystalline defects, Sci. Adv. 2 (12) (2016), doi:10.1126/sciadv.1601796.
[41] S.K. Makineni, A. Kumar, M. Lenz, P. Kontis, T. Meiners, C. Zenk, S. Zaefferer, G. Eggeler, S. Neumeier, E. Spiecker, D. Raabe, B. Gault, On the diffusive phase transformation mechanism assisted by extended dislocations during creep of a single crystal CoNi-based superalloy, Acta Mater. 155 (2018) 362–371, doi:10.1016/j.actamat.2018.05.074.
[42] T.J. Garosshen, G.P. McCarthy, Low-temperature carbide precipitation in a nickel-base superalloy, Metall. Trans. A 16 (7) (1985) 1213–1223.
[43] K.B.S. Rao, V. Seetharaman, S.L. Mannan, P. Rodriguez, Effect of long-term exposure at elevated temperatures on the structure and properties of a nimonic PE 16 superalloy, Mater. Sci. Eng. 58 (1) (1983) 93–106.
[44] M. Sundararaman, P. Mukhopadhyay, S. Banerjee, Carbide precipitation in nickel base superalloys 718 and 625 and their effect on mechanical properties, Superalloys 718 (1997) 625–706.
[45] Q. Wu, H. Song, R.W. Swindeman, J.P. Shingledecker, V.K. Vasudevan, Microstructure of long-term aged IN617 Ni-base superalloy, Metall. Mater. Trans. A 39A (11) (2008) 2569–2585, doi:10.1007/s11661-008-9618-y.
[46] S. Xu, J.I. Dickson, A.K. Koul, Grain growth and carbide precipitation in superalloy, UDIMET 520, Metall. Mater. Trans. A 29 (11) (1998) 2687–2695.
[47] Q.Z. Chen, N. Jones, D.M. Knowles, The microstructures of base/modified RR2072 SX superalloys and their effects on creep properties at elevated temperatures, Acta Mater. 50 (5) (2002) 1095–1112.
[48] P.J. Phillips, R.R. Unocic, L. Kovarik, D. Mourer, D. Wei, M.J. Mills, Low cycle fatigue of a Ni-based superalloy: non-planar deformation, Scr. Mater. 62 (10) (2010) 790–793, doi:10.1016/j.scriptamat.2010.01.044.
[49] P.J. Phillips, R.R. Unocic, M.J. Mills, Low cycle fatigue of a polycrystalline Ni-based superalloy: deformation substructure analysis, Int. J. Fatigue 57 (2013) 50–57, doi:10.1016/j.ijfatigue.2012.11.008.
[50] M. Knop, P. Mulvey, F. Ismail, A. Radecka, K.M. Rahman, T.C. Lindley, B.A. Shollock, M.C. Hardy, M.P. Moody, T.L. Martin, P.A.J. Bagot, D. Dye, A new polycrystalline Co-Ni superalloy, JOM 66 (2014) 2495–2501, doi:10.1007/s11837-014-1175-9.
[51] D. Dye, M. Knop, H.Y. Yan, M.C. Hardy, H.J. Stone, European patent specification EP2821519b1,
[52] L.A. Giannuzzi, F.A. Stevie, A review of focused ion beam milling techniques for TEM specimen preparation, Micron 30 (3) (1999) 197–204.
[53] J. Mayer, L.A. Giannuzzi, T. Kamino, J. Michael, TEM Sample preparation and FIB-induced damage, MRS Bull. 32 (2007) 400–407.
[54] Y.F. Gu, C. Cui, D. Ping, H. Harada, T. Fukuda, J. Fujioka, Creep behavior of new kinds of Ni-Co-base superalloys, Mater. Sci. Eng. A 510-11 (2009) 250–255, doi:10.1016/j.msea.2008.04.128.
[55] K.A. Christofidou, M.C. Hardy, H.Y. Li, C. Argyrakis, H. Kitaguchi, N.G. Jones, P.M. Mignanelli, A.S. Wilson, O.M.D.M. Messé, E.J. Pickering, R.J. Gilbert, C.M.F. Rae, S. Yu, A. Evans, D. Child, P. Bowen, H.J. Stone, On the effect of Nb on the microstructure and properties of next generation polycrystalline powder metallurgy Ni-based superalloys, Metall. Mater. Trans. A 49 (2018) 3896–3907, doi:10.1007/s11661-018-4682-4.
[56] T.P. Gabb, J. Telesman, P.T. Kantzos, K. O'Connor, Characterization of the Temperature Capabilities of Advanced Disk Alloy ME3, NASA, Glenn Research Center, Hannover, USA, 2002. Tech. rep., nasa/tm-2002-2011796
[57] T.M. Smith, B.D. Esser, N. Antolin, A. Carlsson, R.E.A. Williams, A. Wessman, T. Hanlon, H.L. Fraser, W. Windl, D.W. McComb, M.J. Mills, Phase transformation strengthening of high-temperature superalloys, Nat. Commun. 7 (2016) 13434, doi:10.1038/ncomms13434.